Available online at www.sciencedirect.com
SCIENCE DIRECT®
Journal of Computational Physics 197 (2004) 540–554
JOURNAL OF COMPUTATIONAL PHYSICS
www.elsevier.com/locate/jcp

An integro-differential formulation for magnetic induction in bounded domains: boundary element–finite volume method

A.B. Iskakov [a], S. Descombes [b], E. Dormy [a,c,*]

[a] *IPGP, 4 Place Jussieu, 75252 Paris Cedex 05, France*
[b] *UMPA, ENS Lyon, 46 allée d'Italie, 69364 Lyon Cedex 07, France*
[c] *CNRS, France*

Received 10 October 2003; received in revised form 10 December 2003; accepted 10 December 2003
Available online 23 January 2004

Abstract

Simulations of magnetohydrodynamic (MHD) flows in bounded domains using spectral methods suffer from a number of serious limitations. Alternative methods based on local discretization raise the problem of how to implement non-local boundary conditions for the magnetic field. We have developed a new strategy for the numerical solution of MHD problems in bounded domains, which combines the flexibility of a local discretization with a rigorous formulation of magnetic boundary conditions next to an insulator in arbitrary geometries. In accordance with the character of underlying equations we apply a global integral approach at the boundary and a differential approach inside the conducting domain. The formulation of the boundary problem in terms of primitive variables allows us to combine these approaches and propose a mixed finite volume and boundary element method. We illustrate its efficiency on magnetic diffusion problems in a sphere and in a finite cylinder.

Keywords: Magnetohydrodynamics and electrohydrodynamics; Hydrodynamic and hydromagnetic problems; Boundary element methods

1. Physical motivation

The self-excited dynamo theory is widely accepted to be the only plausible explanation for the existence of a large scale planetary magnetic field, as we have on Earth. It is also expected to account for the large scale field in stars, like the Sun, and galaxies as well [1]. Self-excited dynamo action involves motions of an electric conductor which amplify and regenerate a magnetic field, overcoming the effects of diffusion. While several early models were proposed that demonstrated this instability in simple devices with properly

* Corresponding author.
E-mail address: dormy@ipgp.jussieu.fr (E. Dormy).

0021-9991/$ - see front matter
doi:10.1016/j.jcp.2003.12.008

arranged wires [2], natural dynamos proved extremely difficult to tackle because they occur in a uniformly connected volume of conducting fluid. Numerical modeling is thus a necessary tool to progress on these issues.

An important issue in dynamo modeling is the non-local nature of the magnetic boundary conditions next to an insulator. Proper matching of the magnetic induction at the boundaries with an outer potential field can be derived in the spectral domain, making use of the appropriate eigenfunctions. Such is the case for modeling perfectly spherical bodies, using spherical harmonic expansions (see for example the international benchmark in [3] and references therein). However, the spectral approach has a number of limitations. First, it is not easily adaptable to more complicated domains. Indeed, when resolving the induction equation in a cylinder to study an experimental setup of the Karlsruhe experiment, Tilgner [4] immersed the cylindrical domain in a large sphere to satisfy the boundary conditions. Even when the boundary of the domain is a sphere, using spherical harmonics can appear as a limitation. The low viscosity in natural flows introduces very sharp shear layers [5–7], which despite of their local nature need an extremely high global resolution to be properly resolved in the spectral domain. This limits the parameter space that can be investigated with spectral approaches. Even worse, theoretical models can be proposed for the geodynamo by dropping the viscous term as well as inertia, and investigating the principal balance between the Lorentz force and the Coriolis term [8]. The resulting system being nonviscous allows discontinuities in the flow. In this case, using spectral methods results in Gibbs oscillations, regardless of the resolution. Another practical aspect mentioned in [9] is that the spherical harmonics expansion is not well suited for massive parallel simulations because of the significant number of communications required for the computation of nonlinear terms. The construction of appropriate magnetic boundary conditions with a local discretization would overcome many of these limitations.

The natural alternatives to spectral methods are the finite element and finite volumes methods (FEM, FVM), widely used in fluid mechanics. They provide robust and accurate solutions for arbitrary geometries. However major difficulties were raised by previous authors in applying these methods to MHD flows [9,10]. The main issue in bounded domains is the conflict between local discretization and the global form of the magnetic boundary conditions. Studies are therefore often performed in periodic domains [11–13] or using somewhat arbitrary boundary conditions [14,15]. Another aspect is the requirement to ensure the field remains divergence free for all time.

A few attempts have already been made to apply the finite element method to the geodynamo and overcome the difficulties mentioned above. Chan et al. [10] studied a spherical α^2-dynamo problem. They constructed approximate boundary conditions for the core-mantle boundary by extending the domain of computation, and introduced an auxiliary pressure to the magnetic induction equation to achieve divergence free solutions. Matsui and Okuda [9] have developed a three-dimensional MHD code for geodynamo simulations. They also extended the computational domain into the external insulator to address the boundary condition issue, but applied a vector potential method to make this approach more rigorous and obtain divergence free solutions.

To address the difficulty of non-local boundary conditions in another way, the integral equation approach was recently proposed as an alternative to the differential equation methods [16,17]. The authors introduce an integral formulation for a mean field dynamo problem. This allows one to naturally match the boundary conditions. The integral problem is resolved through a classical poloidal–toroidal decomposition of vector fields followed by a spherical harmonic expansion. This approach is found to be extremely accurate in the case of well chosen α and without any large scale flow. This formulation is however difficult to generalize to arbitrary time dependent velocity fields, since it relies on a volume integration involving the electric field at each time step. The approach is also intrinsically limited to the kinematic dynamo problem and will not be extendable to the full set of non-linear coupled equations of the MHD system.

Two alternative approaches to resolve magnetic induction boundary conditions without expansion into spherical functions have been proposed in [18,19]. These are discussed and compared by Pavel Hejda [20].

Both approaches are essentially based on poloidal–toroidal decomposition for the magnetic and velocity fields (**B** and **u**). In the exterior of the sphere the toroidal component of the magnetic field vanishes. The poloidal part is governed by an outer elliptic problem with Dirichlet boundary conditions. In Jepps' method [18] this exterior problem is reduced to the internal one and solved inside the sphere. In Ivanova's method [19] it is solved with the aid of Green function formalism. In both cases the linear integral operator for the poloidal part of the magnetic induction on the boundary can be computed and used to timestep the finite difference system. The poloidal–toroidal decomposition can easily be used for kinematic problems in two dimensions. However in the general case of arbitrary three-dimensional flows, the term $\mathbf{u} \times \mathbf{B}$ in the induction equation is not divergence free and cannot be decomposed in a poloidal and a toroidal part. Therefore the resulting formulation for both the induction equation and the Navier–Stokes equation expressed for the poloidal and toroidal components includes at least fourth-order terms in space and requires the systematic inversion of the horizontal Laplacian operator. This becomes a non-trivial and highly diffusive task with non-spectral methods. Therefore the approaches discussed in [18–20] cannot be easily extended to general three-dimensional flows.

The problem of non-local magnetic conditions can also occur in plasma physics when the stability of a plasma in tokomaks is investigated. This problem, although different, bares some similarity to the one we will investigate here. A solution has been proposed [21,22] by using Green's theorem for a problem with axisymmetric boundaries of arbitrary cross-sections. The stability of the resulting system is then investigated in spectral space rather than with a local discretization as we will propose here.

To summarize, a proper implementation of magnetic boundary conditions with an insulating exterior remains the principal limitation to the development of new codes for natural dynamos using non-spectral methods (finite volume, finite elements, spectral elements, etc.). In this article, we develop a new strategy for the numerical resolution of MHD problems in bounded domains. We apply an integral formulation on the boundary where the magnetic field has a global nature, and combine it with a local discretization inside the domain. In contrast to the methods discussed in [20] our approach does not require a poloidal–toroidal decomposition, and it provides solutions in terms of primitive variables. It is therefore not restricted to special types of flows and allows arbitrary three-dimensional configurations. In terms of numerical strategy, we propose to couple finite volumes and boundary elements. This allows a rigorous formulation of the global boundary conditions in arbitrary geometries and provides an efficient and convenient method for parallel computations.

In Section 2, we describe the finite volume formulation in the context of the kinematic dynamo problem (i.e. for a specified velocity field) and introduce the divergence free update of the magnetic field. In Section 3, the boundary problem is formulated in terms of primitive variables. In Section 4 we solve this problem by introducing the integral approach on the boundary together with the boundary element method. Finally, we present some numerical examples of magnetic diffusion problems in a sphere as well as in a finite cylinder to demonstrate the efficiency of this formulation. In conclusion some remarks on practical applications of this technique are given.

2. Finite volume formulation

The behavior of the magnetic field in the MHD approximation is governed by the magnetic induction equation which neglects the free charge density and the displacement current. In a medium of electrical conductivity σ this equation is

$$\frac{\partial \mathbf{B}}{\partial t} = \nabla \times (\mathbf{u} \times \mathbf{B}) + \eta \Delta \mathbf{B}, \tag{1}$$

where $\eta = (\mu_0\sigma)^{-1}$. It can be expressed in non-dimensional form introducing the magnetic Reynolds number $Rm = UL/\eta$, and using the diffusive time scale, L^2/η, as unit of time

$$\frac{\partial \mathbf{B}}{\partial t} = Rm\nabla \times (\mathbf{u} \times \mathbf{B}) + \Delta \mathbf{B}. \tag{2}$$

We choose this scaling because numerical examples will be performed in the limit $Rm \to 0$. When interested in fast dynamos (limit of infinite Rm), it is customary to use the advective time scale instead (i.e. L/U) which results in a coefficient Rm^{-1} in front of the diffusion term. The magnetic field also satisfies the divergence free condition

$$\nabla \cdot \mathbf{B} = 0. \tag{3}$$

Introducing the electric field

$$\mathbf{E} = -Rm(\mathbf{u} \times \mathbf{B}) + \nabla \times \mathbf{B}, \tag{4}$$

the induction equation (2) can be represented in conservative form by Faraday's law

$$\frac{\partial \mathbf{B}}{\partial t} = -\nabla \times \mathbf{E}. \tag{5}$$

Eq. (5) implies that condition (3) remains valid for all times provided it was satisfied initially, i.e.

$$\frac{\partial}{\partial t}(\nabla \cdot \mathbf{B}) = 0. \tag{6}$$

It is not a trivial matter to obtain a discrete analog of Eqs. (4)–(6). We refer the reader to [23] for an extensive discussion and comparison of the different strategies. Since we are interested in resistive MHD, following [24] (see also [11]) we will use the constrained transport algorithm (CTA). The computational domain is divided into control volumes. The three components of the magnetic field are collocated at the centers of the volume's faces to which they are orthogonal. In this case the magnetic field is to be interpreted as an area-weighted average on the cell face. The components of the electric fields are collocated at the volume's edges to which they are parallel. As a result the different components of the magnetic and electric fields are collocated at different spatial points in the control volumes as represented in Fig. 1. The control volume centers are indexed by (i, j, k). Variables defined at the volume faces will have one half-integer index. Variables defined at the edges will be marked by two half integer indices.

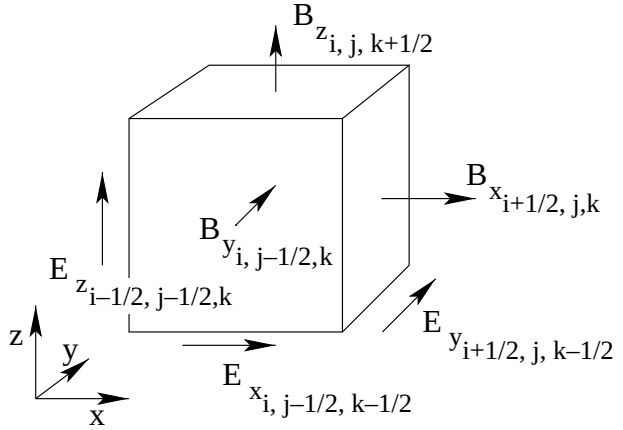

Fig. 1. The staggered mesh used for computing the magnetic and electric fields according to the constrained transport algorithm.

According to Stokes' theorem the rate of change of the magnetic flux across a given face of area S_{face} is taken as a minus circulation of the electric field around the face contour C_{face} (see Fig. 2):

$$\int_{S_{\text{face}}} \frac{\partial B_n}{\partial t} \mathrm{d}s = -\int_{S_{\text{face}}} (\nabla \times \mathbf{E}) \cdot \mathbf{n} \, \mathrm{d}s = -\oint_{C_{\text{face}}} \mathbf{E} \cdot \mathrm{d}\mathbf{l}, \tag{7}$$

and the standard finite volume approach yields for the mean flux

$$\frac{\mathrm{d}B_n}{\mathrm{d}t} S_{\text{face}} = -\oint_{C_{\text{face}}} \mathbf{E} \cdot \mathrm{d}\mathbf{l}. \tag{8}$$

Introducing S_x, S_y, S_z as the face areas and l_x, l_y, l_z as the edge lengths, the approximated contour integrals yield the finite volume analog of Faraday's law (5)

$$\begin{aligned}
-S_{x,i-1/2,j,k} \cdot \frac{B^{n+1}_{x,i-1/2,j,k} - B^{n}_{x,i-1/2,j,k}}{\Delta t} &= (l_y \cdot E_y^{n+1/2})_{i-1/2,j,k-1/2} - (l_y \cdot E_y^{n+1/2})_{i-1/2,j,k+1/2} \\
&\quad - (l_z \cdot E_z^{n+1/2})_{i-1/2,j-1/2,k} + (l_z \cdot E_z^{n+1/2})_{i-1/2,j+1/2,k}, \\
-S_{y,i,j-1/2,k} \cdot \frac{B^{n+1}_{y,i,j-1/2,k} - B^{n}_{y,i,j-1/2,k}}{\Delta t} &= (l_z \cdot E_z^{n+1/2})_{i-1/2,j-1/2,k} - (l_z \cdot E_z^{n+1/2})_{i+1/2,j-1/2,k} \\
&\quad - (l_x \cdot E_x^{n+1/2})_{i,j-1/2,k-1/2} + (l_x \cdot E_x^{n+1/2})_{i,j-1/2,k+1/2}, \\
-S_{z,i,j,k-1/2} \cdot \frac{B^{n+1}_{z,i,j,k-1/2} - B^{n}_{z,i,j,k-1/2}}{\Delta t} &= (l_x \cdot E_x^{n+1/2})_{i,j-1/2,k-1/2} - (l_x \cdot E_x^{n+1/2})_{i,j+1/2,k-1/2} \\
&\quad - (l_y \cdot E_y^{n+1/2})_{i-1/2,j,k-1/2} + (l_y \cdot E_y^{n+1/2})_{i-1/2,j,k-1/2}.
\end{aligned} \tag{9}$$

These equations can also be written in an operator form

$$\frac{\mathbf{B}^{n+1} - \mathbf{B}^{n}}{\Delta t} = -\mathbf{Curl}\, \mathbf{E}^{n+1/2}, \tag{10}$$

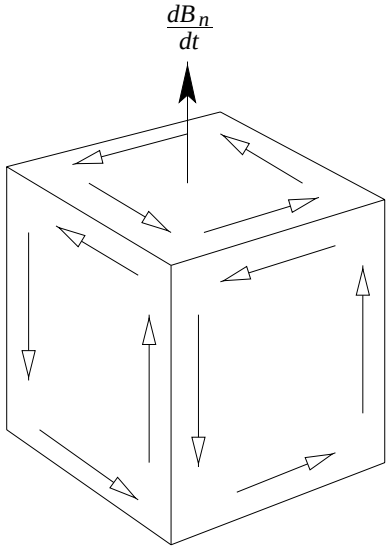

Fig. 2. Divergence free magnetic induction update according to Stokes' theorem.

where **Curl** is an operator which reflects a vector field defined at the volume's edges into a vector field defined on the volume's faces according to (9).

As a consequence of (8) the magnetic flux F_{cell} out of the control volume remains zero provided that it was so initially

$$\frac{\mathrm{d}F_{\text{cell}}}{\mathrm{d}t} = \sum_{\text{faces}} \left(\frac{\mathrm{d}B_n}{\mathrm{d}t} \right)_i S_i = -\sum_{\text{faces}} \oint_{C_i} \mathbf{E}\,\mathrm{d}\mathbf{l} = 0. \tag{11}$$

The last identity is exactly satisfied at the discrete level because the integral of the electric field along each volume's edge is taken twice in opposite directions (see Fig. 2).

Eq. (11) provides a discrete analog of the divergence free condition (6) and ensures the solenoidal character of the magnetic field through the computation.

In order to derive the finite volume scheme for the electric field according to (4), we divide it into an inductive part and a resistive part:

$$\mathbf{E} = -Rm(\mathbf{u} \times \mathbf{B}) + \nabla \times \mathbf{B} = \hat{\mathbf{E}}_{\text{induct}} + \tilde{\mathbf{E}}_{\text{resist}}. \tag{12}$$

To calculate the resistive part in (12) on a general grid one has to construct the dual operator Curl* conjugate to operator Curl in the sense of the support-operators [25,26]

$$\tilde{\mathbf{E}}^{n+1/2} = \frac{1}{2}(\mathbf{Curl}^* \mathbf{B}^{n+1} + \mathbf{Curl}^* \mathbf{B}^n). \tag{13}$$

This operator reflects a vector field defined on the volume faces into a vector field defined at the edges. It is derived from the condition that it should satisfy the discrete analog of the integral vector identity

$$\int_V \mathbf{E} \cdot \mathbf{Curl}^* \mathbf{B}\,\mathrm{d}V - \int_V \mathbf{B} \cdot \mathbf{Curl}\,\mathbf{E}\,\mathrm{d}V = \int_S (\mathbf{E} \times \mathbf{B}) \cdot \mathbf{n}\,\mathrm{d}s, \tag{14}$$

on a given grid for arbitrary vector fields **E** and **B**.

The determination of this dual operator can in fact be related to the traditional issue of the proper construction of a dual mesh in staggered finite volumes (e.g. [27]). The support-operators approach here provides a systematic way to construct this mesh.

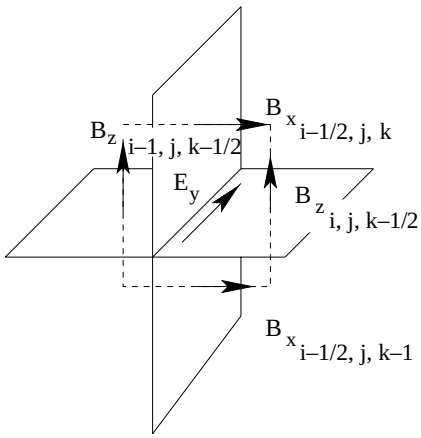

Fig. 3. Evaluation of the circulation of B along the path enclosing the edges to calculate the tangent component of E on the edge.

On a regular cartesian, cylindrical or spherical computational mesh, the dual operator can be easily derived. Simply connecting neighboring volume centers provides the integration contours for the dual mesh (see Fig. 3). The resistive part of the electric field $\tilde{\mathbf{E}}$ can then be obtained by Stokes' theorem as a circulation of the magnetic field $\mathbf{B}$ around these contours

$$\tilde{E}^{n+1/2}_{\text{face}} \cdot \tilde{S}_{\text{face}} = \frac{1}{2} \oint_{\tilde{C}_{\text{face}}} (\mathbf{B}^{n+1} + \mathbf{B}^{n}) \cdot \mathrm{d}\mathbf{l}. \tag{15}$$

Denoting by $\tilde{S}_x, \tilde{S}_y, \tilde{S}_z$ contour areas and by $\tilde{l}_x, \tilde{l}_y, \tilde{l}_z$ lengths of their sides, we obtain the finite volume scheme for the resistive part of the electric flux

$$\begin{aligned}
(\tilde{S}_x \tilde{E}_x^{n+1/2})_{i,j-1/2,k-1/2} &= \begin{pmatrix} (\tilde{l}_y B_y^{n+1/2})_{i,j-1/2,k-1} - (\tilde{l}_y B_y^{n+1/2})_{i,j-1/2,k} \\ -(\tilde{l}_z B_z^{n+1/2})_{i,j-1,k-1/2} + (\tilde{l}_z B_z^{n+1/2})_{i,j,k-1/2} \end{pmatrix}, \\
(\tilde{S}_y \tilde{E}_y^{n+1/2})_{i-1/2,j,k-1/2} &= \begin{pmatrix} (\tilde{l}_z B_z^{n+1/2})_{i-1,j,k-1/2} - (\tilde{l}_z B_z^{n+1/2})_{i,j,k-1/2} \\ -(\tilde{l}_x B_x^{n+1/2})_{i-1/2,j,k-1} + (\tilde{l}_x B_x^{n+1/2})_{i-1/2,j,k} \end{pmatrix}, \\
(\tilde{S}_z \tilde{E}_z^{n+1/2})_{i-1/2,j-1/2,k} &= \begin{pmatrix} (\tilde{l}_x B_x^{n+1/2})_{i-1/2,j-1,k} - (\tilde{l}_x B_x^{n+1/2})_{i-1/2,j,k} \\ -(\tilde{l}_y B_y^{n+1/2})_{i-1,j-1/2,k} + (\tilde{l}_y B_y^{n+1/2})_{i,j-1/2,k} \end{pmatrix},
\end{aligned} \tag{16}$$

where $\mathbf{B}^{n+1/2} = \frac{1}{2}(\mathbf{B}^n + \mathbf{B}^{n+1})$.

When the magnetic Reynolds number Rm is moderate, the inductive part of the electric field $\hat{\mathbf{E}}$ could be evaluated by simply interpolating $\mathbf{u} \times \mathbf{B}$ on the edges. On a uniform cartesian mesh $\hat{\mathbf{E}}$ would then be taken as an average of the appropriate values defined at the faces

$$\begin{aligned}
\hat{E}^{n+1/2}_{x,i,j-1/2,k-1/2} &= \frac{Rm}{2} \begin{pmatrix} (B_y \cdot u_z)^{n+1/2}_{i,j-1/2,k-1} + (B_y \cdot u_z)^{n+1/2}_{i,j-1/2,k} \\ -(B_z \cdot u_y)^{n+1/2}_{i,j-1,k-1/2} - (B_z \cdot u_y)^{n+1/2}_{i,j,k-1/2} \end{pmatrix}, \\
\hat{E}^{n+1/2}_{y,i-1/2,j,k-1/2} &= \frac{Rm}{2} \begin{pmatrix} (B_z \cdot u_x)^{n+1/2}_{i-1,j,k-1/2} + (B_z \cdot u_x)^{n+1/2}_{i,j,k-1/2} \\ -(B_x \cdot u_z)^{n+1/2}_{i-1/2,j,k-1} - (B_x \cdot u_z)^{n+1/2}_{i-1/2,j,k} \end{pmatrix}, \\
\hat{E}^{n+1/2}_{z,i-1/2,j-1/2,k} &= \frac{Rm}{2} \begin{pmatrix} (B_x \cdot u_y)^{n+1/2}_{i-1/2,j-1,k} + (B_x \cdot u_y)^{n+1/2}_{i-1/2,j,k} \\ -(B_y \cdot u_x)^{n+1/2}_{i-1,j-1/2,k} - (B_y \cdot u_x)^{n+1/2}_{i,j-1/2,k} \end{pmatrix}.
\end{aligned} \tag{17}$$

If Rm is large, a proper treatment of the inductive part $\hat{\mathbf{E}}$ is needed. Particularly, in the full MHD simulations, $\hat{\mathbf{E}}$ can be calculated through the fluxes obtained from a higher order MHD Godunov scheme (see [11,12]). For simplicity and since the inductive term does not raise special difficulties with the boundary conditions, we will restrict our analysis to the case of low Rm for which a simple interpolation (17) is suitable.

Eqs. (9), (12), (16) and (17) provide the finite volume formulation of the induction equations (4) and (5).

3. Boundary formulation

The finite volume scheme described in the previous section is not self-consistent if the computational domain Ω is bounded. To apply it directly to MHD flows in bounded domain one needs to formulate magnetic boundary conditions in terms of primitive variables using a local discretization.

The finite volume scheme (9), (12), (16), (17) requires expressions for the tangential components of the electric field at the boundary through the magnetic field. Let us assume that the boundary Γ is fixed in time and is rigid, so that the velocity $\mathbf{u}$ has no normal component on Γ:

$$\mathbf{u}_\Gamma \cdot \mathbf{n} = 0. \tag{18}$$

The tangential component of the electric field along the unit vector $\boldsymbol{\tau}$ at the boundary according to (4) is then

$$E_\tau = -Rm\,\boldsymbol{\tau} \cdot (\mathbf{u} \times (B_n \mathbf{n})_\Gamma) + \boldsymbol{\tau} \cdot (\nabla \times \mathbf{B})_\Gamma, \tag{19}$$

where $\mathbf{n}$ is the unit outward normal on the boundary, B_n is the component of $\mathbf{B}$ along $\mathbf{n}$, E_τ is the component of $\mathbf{E}$ along $\boldsymbol{\tau}$, and

$$(\nabla \times \mathbf{B})_\Gamma = \lim_{\substack{\mathbf{r} \to \Gamma \\ \mathbf{r} \in \Omega}} (\nabla \times \mathbf{B}(\mathbf{r})). \tag{20}$$

The first term in (19) obviously requires knowledge of B_n only and thus raises no special difficulty. In contrast, to approximate the limit (20), one needs to know the tangential component of the magnetic field on Γ. The method of approximation here depends on the particular grid being used.

Let us consider for simplicity a regular orthogonal grid on the boundary with the Z-axis directed along $\mathbf{n}$ (see Fig. 4). Using the notations introduced in the previous section, we estimate the tangential components of the electric field E_x and E_y on Γ according to (19) as

$$\begin{aligned}
E_{x,i,j+1/2,k+1/2} = & -\frac{Rm}{2}\left\{(u_y \cdot B_z)_{i,j,k+1/2} + (u_y \cdot B_z)_{i,j+1,k+1/2}\right\} \\
& + \left\{ -\frac{\tilde{B}_{y,i,j+1/2,k+1/2} - B_{y,i,j+1/2,k}}{\Delta z/2} + \frac{B_{z,i,j+1,k+1/2} - B_{z,i,j,k+1/2}}{\Delta y} \right\}, \\
E_{y,i+1/2,j,k+1/2} = & \frac{Rm}{2}\left\{(u_x \cdot B_z)_{i,j,k+1/2} + (u_x \cdot B_z)_{i+1,j,k+1/2}\right\} \\
& + \left\{ \frac{\tilde{B}_{x,i+1/2,j,k+1/2} - B_{x,i+1/2,j,k}}{\Delta z/2} - \frac{B_{z,i+1,j,k+1/2} - B_{z,i,j,k+1/2}}{\Delta x} \right\},
\end{aligned} \tag{21}$$

where Δx, Δy and Δz are grid steps, $\tilde{B}_x$ and $\tilde{B}_y$ are the tangential components of $\mathbf{B}$ on Γ. The second terms in (21) represent an approximation to the limit (20). To achieve second-order accuracy one has to add, respectively, to the right-hand sides of (21) the additional terms

$$\begin{aligned}
& -\frac{1}{3}\left(\frac{\tilde{B}_{y,i,j+1/2,k+1/2} - B_{y,i,j+1/2,k}}{\Delta z/2} - \frac{B_{y,i,j+1/2,k} - B_{y,i,j+1/2,k-1}}{\Delta z} \right), \\
& \frac{1}{3}\left(\frac{\tilde{B}_{x,i+1/2,j,k+1/2} - B_{x,i+1/2,j,k}}{\Delta z/2} - \frac{B_{x,i+1/2,j,k} - B_{x,i+1/2,j,k-1}}{\Delta z} \right).
\end{aligned} \tag{22}$$

To apply Eq. (21) one needs some additional information on the tangential components of the magnetic field on the boundary, which should be obtained from the boundary conditions. The resulting boundary problem for the finite volume scheme (9), (12), (16), (17), (21) is to calculate the tangential components of the magnetic field on the boundary through its normal component, known on the boundary.

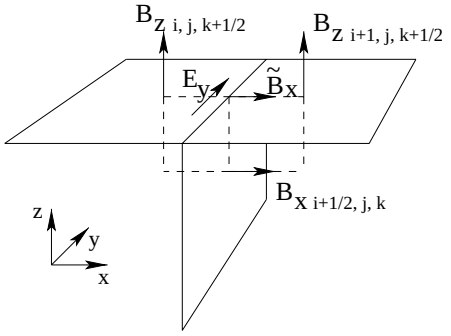

Fig. 4. Estimation of the tangential electric field E_y on the boundary.

4. Integral formulation at the boundary

The boundary problem formulated in the previous section should be solved through the boundary condition that the magnetic field must match a potential field at the boundary. This problem is global, i.e. the tangential component of the magnetic field at a given point depends on the values of its normal component everywhere on the boundary. This dependence is however linear and in this section we construct the appropriate linear operator through an integral formulation.

The problem of matching a potential field can be formulated as an elliptic problem in Ω^c, the complementary domain of Ω:

$$\mathbf{B} = -\nabla\phi, \quad \Delta\phi = 0, \tag{23}$$

where $\phi : \Omega^c \to \mathbb{R}$ is the potential function.

Having in mind the geodynamo problem, we assume further that Ω is bounded and Ω^c is unbounded although the following approach is applicable in other cases as well. At infinity, the physical condition for the magnetic field gives

$$\phi \to \mathrm{O}(r^{-2}), \quad r \to \infty. \tag{24}$$

The normal component of the magnetic field B_n is known on the boundary Γ which implies a Neuman boundary condition on the potential

$$\left.\frac{\partial\phi}{\partial n}\right|_{\Gamma} = -B_n \quad (B_n : \Gamma \to \mathbb{R}). \tag{25}$$

The numerical resolution of the corresponding elliptic problem (23)–(25) by a finite element method (or any other meshed method), involves arbitrarily bounding this domain [9,10]. This introduces additional approximations. In contrast, an integral formulation allows us to tackle this problem directly. Under the framework of an integral approach to the elliptic problem (23), potential field characteristics can be expressed as surface integrals over the appropriate fundamental solution (i.e. the solution of the equation $\Delta G = \delta(\mathbf{x}, \mathbf{y})$)

$$G(\mathbf{x}, \mathbf{y}) = \frac{-1}{4\pi|\mathbf{x} - \mathbf{y}|}. \tag{26}$$

In particular, denoting by $\mathscr{B}_R$ an open ball of radius R such that $\overline{\Omega} \subset \mathscr{B}_R$, as a consequence of Green's theorem the magnetic potential at $\mathbf{x} \in \Gamma$ satisfies [28,29]

$$\phi(\mathbf{x}) = -2\int_\Gamma \left(\phi(\mathbf{y})\frac{\partial G(\mathbf{x},\mathbf{y})}{\partial n} + B_n(\mathbf{y})G(\mathbf{x},\mathbf{y})\right)\mathrm{d}s(\mathbf{y}) + 2\int_{\partial\mathscr{B}_R}\left(\phi(\mathbf{y})\frac{\partial G(\mathbf{x},\mathbf{y})}{\partial \tilde{n}} - \frac{\partial\phi(\mathbf{y})}{\partial\tilde{n}}G(\mathbf{x},\mathbf{y})\right)\mathrm{d}s(\mathbf{y}), \tag{27}$$

where n is the coordinate along the outward normal to Ω and $\tilde{n}$ is the coordinate along the outward normal to $\mathscr{B}_R$. The second term (i.e. the integral over $\partial\mathscr{B}_R$) however vanishes when $R \to +\infty$ (keeping the center of the ball fixed). So we can simply write

$$\phi(\mathbf{x}) = -2\int_\Gamma \left(\phi(\mathbf{y})\frac{\partial G(\mathbf{x},\mathbf{y})}{\partial n} + B_n(\mathbf{y})G(\mathbf{x},\mathbf{y})\right)\mathrm{d}s(\mathbf{y}). \tag{28}$$

Consequently the tangential component of the magnetic field on Γ along the unit vector $\boldsymbol{\tau}$ is

$$B_\tau(\mathbf{x}) = -\boldsymbol{\tau}\cdot\nabla\phi(\mathbf{x}) = 2\boldsymbol{\tau}\cdot\int_\Gamma\left(\phi(\mathbf{y})\nabla_x\frac{\partial G(\mathbf{x},\mathbf{y})}{\partial n} + B_n(\mathbf{y})\nabla_x G(\mathbf{x},\mathbf{y})\right)\mathrm{d}s(\mathbf{y}). \tag{29}$$

The solution of Eqs. (28) and (29) provides the tangential component B_τ on Γ through the normal component B_n. However, to numerically obtain this solution using local discretization, one needs to construct an appropriate discrete analog of these equations. The discrete analog of the integral approach for numerical applications has been developed as the boundary element method (BEM) [28,29].

In the BEM formalism the boundary surface is subdivided into small elements and each element contains several nodes where the boundary variables and conditions are defined. Let us introduce a tessellation of Γ in terms of S_j, i.e. $S_i \cap S_j = O$ ($\forall i, j$ with $i \neq j$), and $\cup_j S_j = \Gamma$. The simplest discrete analog of Eqs. (28) and (29) can then be written as

$$\frac{1}{2}\phi_i = -\sum_j \phi_j \int_{S_j}\frac{\partial G}{\partial n}(\mathbf{x}_i,\mathbf{y})\mathrm{d}s(\mathbf{y}) - \sum_j B_{nj}\int_{S_j} G(\mathbf{x}_i,\mathbf{y})\mathrm{d}s(\mathbf{y}), \tag{30}$$

$$B_{\tau i} = \sum_j \phi_j \int_{S_j} 2\boldsymbol{\tau}\cdot\nabla_x\frac{\partial G}{\partial n}(\mathbf{x}_i,\mathbf{y})\mathrm{d}s(\mathbf{y}) + \sum_j B_{nj}\int_{S_j} 2\boldsymbol{\tau}\cdot\nabla_x G(\mathbf{x}_i,\mathbf{y})\mathrm{d}s(\mathbf{y}), \tag{31}$$

where

$$\phi_i = \phi(\mathbf{x}_i), \quad B_{ni} = B_n(\mathbf{x}_i), \quad B_{\tau i} = B_\tau(\mathbf{x}_i)$$

are potentials and magnetic field components at node i on the boundary, while S_j is the boundary surface corresponding to node j.

If we assemble the potentials ϕ_i and components of the magnetic field B_{ni}, $B_{\tau i}$ defined in all boundary nodes in vectors $\overline{\Phi}$, $\overline{B}_n$ and $\overline{B}_\tau$, the linear systems (30) and (31) can be rewritten in a matrix form

$$\frac{1}{2}\overline{\Phi} = A\overline{\Phi} + C\overline{B}_n, \tag{32}$$

$$\overline{B}_\tau = D\overline{\Phi} + F\overline{B}_n, \tag{33}$$

where A, C, D, and F are matrices with coefficients depending only on the geometry of the computational grid

$$A_{ij} = -\int_{S_j}\frac{\partial G}{\partial n}(\mathbf{x}_i,\mathbf{y})\mathrm{d}s(\mathbf{y}), \quad C_{ij} = -\int_{S_j} G(\mathbf{x}_i,\mathbf{y})\mathrm{d}s(\mathbf{y}), \tag{34}$$

$$D_{ij} = \int_{S_j} 2\boldsymbol{\tau} \cdot \nabla_x \frac{\partial G}{\partial n}(\mathbf{x}_i, \mathbf{y}) \mathrm{d}s(\mathbf{y}), \quad F_{ij} = \int_{S_j} 2\boldsymbol{\tau} \cdot \nabla_x G(\mathbf{x}_i, \mathbf{y}) \mathrm{d}s(\mathbf{y}). \tag{35}$$

Different possible approximations for the matrix coefficients determine the accuracy of the method. Different values can also be defined at different sets of nodes on the boundary.

In general, for each node on the boundary we have two tangential components (two different tangential directions $\boldsymbol{\tau}$) and one normal component. Therefore, if matrices A and C have size of $N \times N$ then matrices D and F have size of $2N \times N$. From the system (32), (33), we obtain a linear, but non-local, expression for the boundary potential $\overline{\Phi}$ and tangential components $\overline{B}_\tau$ through the normal components $\overline{B}_n$:

$$\overline{\Phi} = (Id/2 - A)^{-1} C \cdot \overline{B}_n,$$

so that

$$\begin{aligned} \overline{B}_\tau &= (D(Id/2 - A)^{-1} C + F) \cdot \overline{B}_n, \\ \overline{B}_\tau &= G \cdot \overline{B}_n. \end{aligned} \tag{36}$$

Eqs. (34)–(36) together with the appropriate integral approximations define the matrix of the linear operator G which allows the solution of the boundary problem and provides a closure for the finite volume formulation (9), (12), (16), (17),(21) described in the previous sections.

Let us now discuss the evaluation of integrals (34) and (35) over elements, as this is the most crucial aspect of the numerical implementation of BEM. The main issue lies in the fact that the functions which have to be integrated exhibit singularities at certain points in the elements.

Whereas integrals for the diagonal coefficients C_{ii} in (34) are weakly singular, and can in principle be evaluated using numerical integration, the integrals for the diagonal coefficients A_{ii}, D_{ii} and F_{ii} in (34) and (35) exist only as Cauchy principal values. Since the principal value of the integral F_{ii} is zero one can calculate it by excluding some small ε-vicinity around x_i. To compute the diagonal coefficients A_{ii}, we substitute $\phi \equiv 1$ into (27)

$$\frac{1}{2} = -\int_{\Gamma_\varepsilon} \frac{\partial G}{\partial n}(\mathbf{x}_i, \mathbf{y}) \mathrm{d}s(\mathbf{y}) - \int_{\Gamma - \Gamma_\varepsilon} \frac{\partial G}{\partial n}(\mathbf{x}_i, \mathbf{y}) \mathrm{d}s(\mathbf{y}) + \int_{\partial \mathscr{B}_R} \frac{\partial G}{\partial \tilde{n}}(\mathbf{x}_i, \mathbf{y}) \mathrm{d}s(\mathbf{y}), \tag{37}$$

where Γ_ε is the part of the boundary in the vicinity of $\mathbf{x}_i$, $|\mathbf{x} - \mathbf{x}_i| < \varepsilon$, $\Gamma - \Gamma_\varepsilon$ is the remaining part of the boundary at $|\mathbf{x} - \mathbf{x}_i| \geqslant \varepsilon$. Since the last integral in (37) tends to unity as $R \to \infty$, we obtain

$$-\int_{\Gamma_\varepsilon} \frac{\partial G}{\partial n}(\mathbf{x}_i, \mathbf{y}) \mathrm{d}s(\mathbf{y}) = -\frac{1}{2} + \int_{\Gamma - \Gamma_\varepsilon} \frac{\partial G}{\partial n}(\mathbf{x}_i, \mathbf{y}) \mathrm{d}s(\mathbf{y}). \tag{38}$$

The discrete analog of this relation provides an estimation of the diagonal matrix elements A_{ii},

$$A_{ii} = -\frac{1}{2} - \sum_{j \neq i} A_{ij}. \tag{39}$$

Similar considerations give an estimation for D_{ii},

$$D_{ii} = -\sum_{j \neq i} D_{ij}. \tag{40}$$

Since the numerical mesh will in general not be modified during the simulation, the matrix G in (36) only has to be calculated once. The boundary condition at each time step is then simply reduced to a matrix multiplication. Moreover, if the mesh has a cylindrical symmetry (which is almost always the case for natural dynamos) the matrix G can be significantly reduced in size.

5. Numerical examples

To test the proposed approach, we have developed a three-dimensional code for the kinematic dynamo problem which couples finite volume and boundary element methods as proposed above. For simplicity we have used structured regular spherical and cylindrical grids. In this section, we present some numerical tests with the magnetic Reynolds number set to zero (only the resistive part is considered). This is enough to test the numerical procedure against known eigenfunctions, and demonstrate the flexibility of this approach.

A first test consists of reproducing the analytical solution for the decaying dipole field in a sphere (see Fig. 5(a)). The slowest decaying mode in the spherical geometry is the dipole field (e.g. [30]), which can be expressed in terms of cylindrical Bessel functions

$$\mathbf{B}(t) = \mathbf{B}_0(r,\theta)\mathrm{e}^{-\sigma t} \quad \text{with } \sigma = \frac{\pi^2}{R^2} \tag{41}$$

with $\mathbf{B}_0$ being defined for $r < R$ as

$$\mathbf{B}_0(r,\theta) = \begin{pmatrix} \frac{2\cos\theta J_{3/2}(\pi r/R)}{r^{3/2}} \\ \frac{\sin\theta}{r^{3/2}}\left(J_{3/2}(\pi r/R) - \frac{\pi r}{R}J_{1/2}(\pi r/R)\right) \\ 0 \end{pmatrix}, \tag{42}$$

and for $r > R$ as

$$\mathbf{B}_0(r,\theta) = \begin{pmatrix} \frac{2\cos\theta J_{3/2}(\pi)}{r^{3/2}}\left(\frac{R}{r}\right)^{3/2} \\ \frac{\sin\theta J_{3/2}(\pi)}{r^{3/2}}\left(\frac{R}{r}\right)^{3/2} \\ 0 \end{pmatrix}, \tag{43}$$

where R is the sphere radius, and $J_{1/2}$ and $J_{3/2}$ are the cylindrical Bessel functions. This mode provides an eigenfunction of the diffusion equation

$$\frac{\partial \mathbf{B}}{\partial t} = -\nabla \times \nabla \times \mathbf{B}. \tag{44}$$

In our simulations the decay dipole field rate tends asymptotically with time to a particular value which corresponds to the slowest decaying mode. The time variation of the decay dipole rates are shown in Fig. 6. The decay rate for a unit sphere clearly converges toward to the analytical dipole decay rate $-\pi^2$ as the resolution is increased. At a resolution of $40 \times 40 \times 40$, the relative error is already approximately 0.1%.

The comparison between radial profiles of meridional and radial components of the magnetic field in the analytical and numerical diffusive solutions after one decaying period is represented in Fig. 7. For a coarse

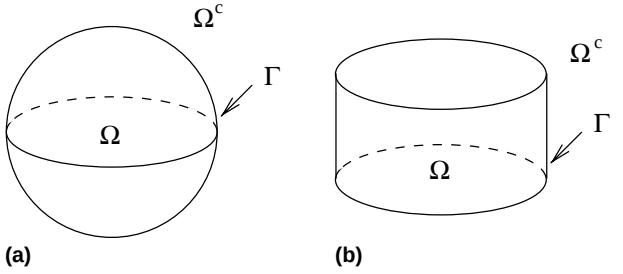

Fig. 5. Computational domains and boundaries for the presented examples: a sphere (a) and a bounded cylinder (b).

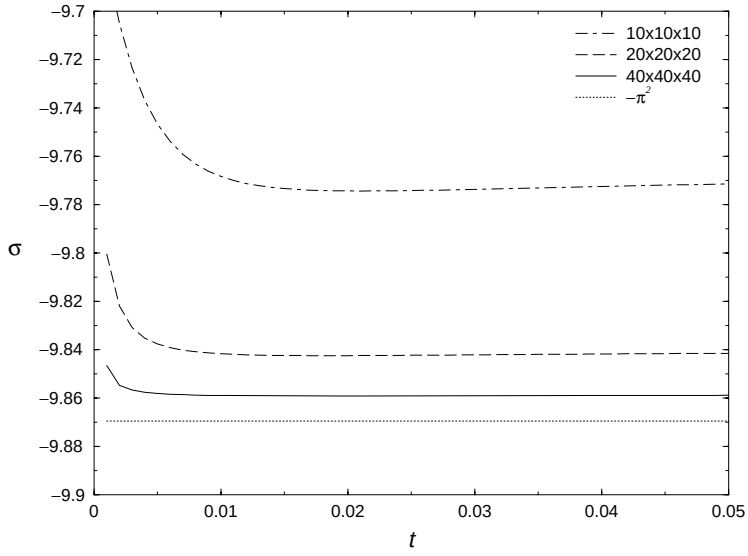

Fig. 6. Decay rate of the computed dipole field for various mesh size. The convergence to the analytical value $-\pi^2$ is demonstrated with increasing resolutions.

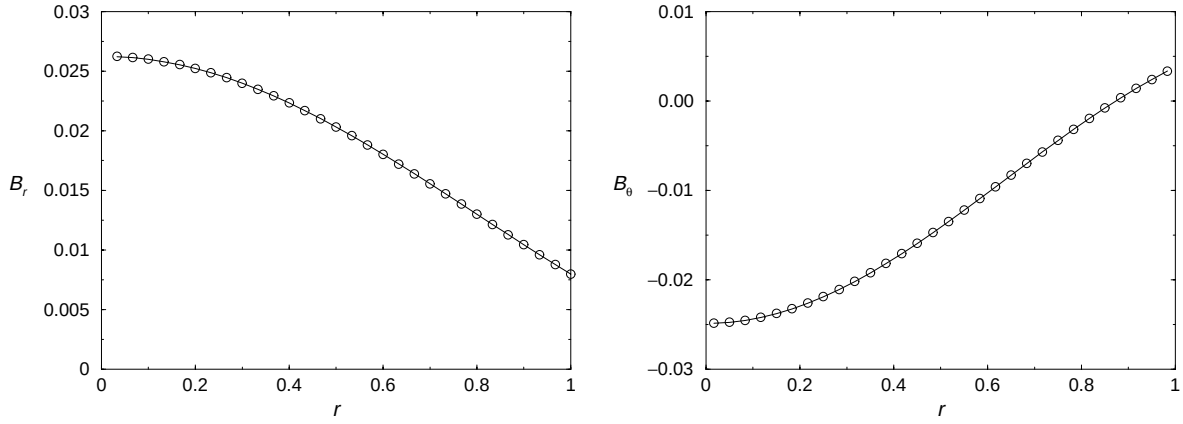

Fig. 7. Cross-sections of the slowest decaying mode (diffusive solution) in a numerical simulation with a coarse grid ($30 \times 30 \times 30$). The numerical solution is here represented with circles, while the analytical solution is plotted with solid lines.

grid of $30 \times 30 \times 30$ the difference is already imperceptible. This demonstrates the efficiency of the mixed finite volume and boundary element method at properly matching the potential field outside the computational domain.

To demonstrate the validity of this approach in an arbitrary geometry, we have calculated the decaying magnetic field in a conducting cylinder of unit height and radius (see Fig. 5(b)). The kinematic dynamo simulation in a similar cylindrical configuration (relevant to an experimental setup) by spectral methods required the extension of the computational domain outside the cylinder to an arbitrary sphere, at which the boundary condition was met [4].

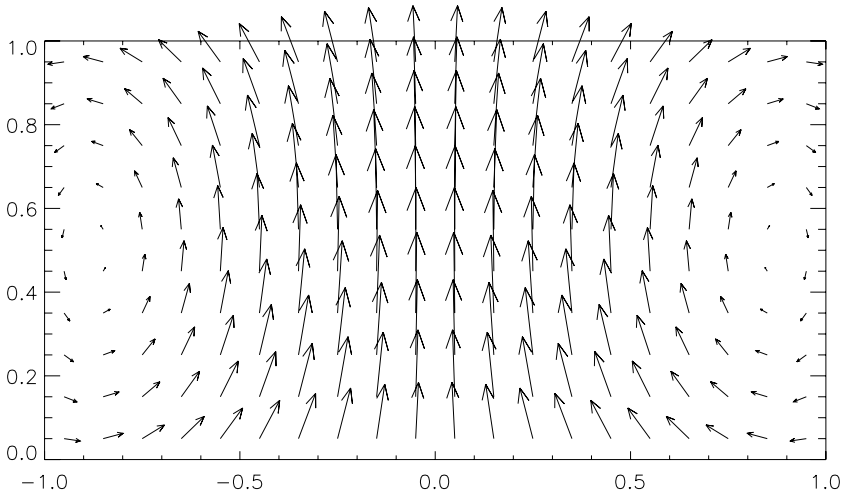

Fig. 8. First decay mode in a bounded cylinder of unit radius and height (the simulation is three-dimensional and the mesh is only $20 \times 20 \times 20$).

The computed magnetic field is axisymmetric (although the simulation is fully three-dimensional) and the solution is represented in a cross section in Fig. 8. It corresponds to the slowest decaying mode in this finite cylinder.

6. Conclusions

The combination of an integral boundary element method with a local differential approach inside the computational domain, reflects the physical nature of underlying equations for magnetic induction. It allows the development of an efficient strategy for modeling the induction equation in arbitrary bounded domains. In terms of the local finite volume approach, the global boundary problem for the magnetic field can be formulated as the estimation of the tangential components of the magnetic field on the boundary through the normal component. Then, utilizing an integral formulation, the non-local boundary conditions can be naturally described as a global linear operator on the boundary. In contrast with [19], our integral formulation provides solution in primitive variables and does not require a poloidal–toroidal decomposition of vector fields. An important characteristic of the boundary operator is its dependence only on the geometry of the bounding surface. So if the boundary does not change in time during the simulation, it is possible to calculate this operator only once for the particular numerical grid, and then use it throughout the numerical simulation. Following this approach we have developed a finite volume scheme, and illustrated its efficiency on magnetic diffusion problems.

To conclude, we would like to highlight some practical applications of this approach. Massive parallel computations, which have become increasingly common during the last few years, reveal limitations in spectral methods which involve a significant number of global operations. The calculation of new magnetic field values at a given point on the boundary surface requires information on the magnetic field over the whole surface, which is unavoidable for a global boundary condition. This inevitably requires some communications in terms of parallel computing. However within the framework of the proposed integral formulation, such transfers are limited to boundary values (in contrast to information in the volume) and thus minimized. In addition, these transfers can be further reduced if the boundary points are treated by a

small number of processors. The approach advocated here therefore provides a correct treatment of the boundary conditions, and is suitable for parallel computations.

References

[1] A. Ferriz-Mas, M. Núñez Jiménez, Advances in nonlinear dynamos, in: Soward, Ghil (Eds.), The Fluid Mechanics of Astrophysics and Geophysics Series, Taylor & Francis, London, 2003.
[2] E.C. Bullard, The stability of a homopolar dynamo, Proc. Cambridge Philos. Soc. 51 (1955) 744–760.
[3] U.R. Christensen, J. Aubert, P. Cardin, E. Dormy, S. Gibbons, G.A. Glatzmaier, E. Grote, H. Honkura, C. Jones, M. Kono, M. Matsushima, A. Sakuraba, F. Takahashi, A. Tilinger, J. Wicht, K. Zhang, A numerical dynamo benchmark, Phys. Earth Planet. Int. 128 (2001) 25–34.
[4] A. Tilgner, Numerical simulation of the onset of dynamo action in an experimental two-scale dynamo, Phys. Fluids 14 (2002) 11.
[5] K. Stewartson, On almost rigid rotations, J. Fluid Mech. 3 (1957) 299–303.
[6] I. Proudman, The almost-rigid rotation of viscous fluid between concentric spheres, J. Fluid Mech. 1 (1956) 505–516.
[7] E. Dormy, D. Jault, A. Soward, A super-rotating shear layer in magnetohydrodynamic spherical Couette flow, J. Fluid Mech. 452 (2002) 263–291.
[8] J.B. Taylor, The magneto-hydrodynamics of a rotating fluid and the Earth's dynamo problem, Proc. R. Soc. Lond. A 274 (1963) 274–283.
[9] H. Matsui, H. Okuda, Development of a simulation code for MHD dynamo processes using the GeoFEM platform, Int. J. Comput. Fluid Dynamics (2004), in press.
[10] K. Chan, K. Zhang, J. Zou, G. Schubert, A non-linear 3D spherical α^2 dynamo using a finite element method, Phys. Earth Planet. Int. 128 (2001) 35–50.
[11] D. Balsara, D. Spicer, A staggered mesh algorithm using high order Godunov fluxes to ensure solenoidal magnetic fields in magnetohydrodynamic simulations, J. Comput. Phys. 149 (1999) 270–292.
[12] D. Balsara, Divergence-free adaptive mesh refinement for magneto-hydrodynamics, J. Comput. Phys. 174 (2001) 614–648.
[13] V. Archontis, S.B.F. Dorch, A. Nordlund, Numerical simulations of kinematic dynamo action, A&A 397 (2003) 393–399.
[14] A. Kageyama, M. Ochi, T. Sato, Flip-flop transitions of the magnetic intensity and polarity reversals in the magnetohydrodynamic dynamo, Phys. Rev. Lett. 62 (26) (1999) 5409–5412.
[15] G. Rüdiger, Y. Zhang, MHD instability in differentially-rotating cylindric flows, A&A 378 (2001) 302–308.
[16] F. Stefani, G. Gerbeth, K.-H. Rädler, Steady dynamos in finite domains: an integral equation approach, Astron. Nachr. 321 (2000) 65–73.
[17] M. Xu, F. Stefani, G. Gerbeth, The integral equation method for a steady kinematic dynamo problem, J. Comput. Phys. (2004), in press.
[18] S.A. Jepps, Numerical models of hydromagnetic dynamos, J. Fluid Mech. 67 (part 4) (1975) 625–646.
[19] T.S. Ivanova, A method for solving hydromagnetic dynamo problem, J. Comput. Math. Math. Phys. 16 (4) (1976) 956–968 (in Russian).
[20] P. Hejda, Boundary conditions in the hydromagnetic dynamo problem, Stud. Geophys. Geod. 26 (1982) 361–372.
[21] D.A. D'Ippolito, J.P. Freidberg, J.P. Goedbloed, J. Rem, High-beta tokamaks surrounded by force-free fields, Phys. Fluids 21 (9) (1978) 1600–1616.
[22] J.P. Freidberg, W. Grossmann, Magnetohydrodynamic stability of a sharp boundary model of tokamak, Phys. Fluids 18 (11) (1975) 1494–1506.
[23] G. Tóth, The $\nabla \cdot B = 0$ constraint in shock-capturing magnetohydrodynamics codes, J. Comput. Phys. 161 (2000) 605–652.
[24] K. Yee, Numerical solution of initial boundary value problems involving Maxwell's equations in isotropic media, IEEE Trans. Antenna Propagation AP-14 (1966) 302.
[25] A.A. Samarskii, V.F. Tishkin, A.P. Favorskii, M.Yu. Shashkov, Operational finite-difference schemes, Differential Equations 17 (7) (1981) 854–862.
[26] M. Shashkov, Conservative Finite-Difference Methods on General Grids, CRC Press, Boca Raton, FL, 1996, pp. 47–149.
[27] E. Dormy, A. Tarantola, Numerical simulation of elastic wave propagation using a finite volume method, J. Geophys. Res. 100 (1995) 2123–2133.
[28] G. Beer, Programming the Boundary Element Method. An Introduction for Engineers, Wiley, New York, 2001.
[29] M. Bonnet, Equations intégrales et éléments de frontière, CNRS Editions/Editions Eyrolles, 1995.
[30] H.K. Moffatt, Magnetic Field Generation in Electrically Conducting Fluids, Cambridge University Press, Cambridge, MA, 1978.